Catalysis Today 183 (2012) 136–142

Contents lists available at SciVerse ScienceDirect

Catalysis Today

journal homepage: www.elsevier.com/locate/cattod

Aqueous phase Fischer–Tropsch synthesis in a continuous flow reactor

Lingtao Liu, Geng Sun, Chen Wang, Jinghe Yang, Chaoxian Xiao, Hang Wang, Ding Ma*, Yuan Kou

PKU Green Chemistry Center, Beijing National Laboratory for Molecular Sciences, College of Chemistry and Molecular Engineering, Peking University, Beijing 100871, China

ARTICLE INFO

Article history:
Received 8 August 2011
Received in revised form
27 September 2011
Accepted 27 September 2011
Available online 19 October 2011

Keywords:
Fischer–Tropsch synthesis
Aqueous phase
Ruthenium
Flow system
Poly(N-vinyl-2-pyrrolidone)

ABSTRACT

Aqueous phase Fischer–Tropsch synthesis catalyzed by Ru nanoparticles was studied in a continuous flow reactor for the first time. A 60 ml autoclave was used for catalyst screening and a 1000 ml reactor was used to test the scale-up stability of the catalysts. Ru nanoparticles reduced by hydrogen in the presence of poly(N-vinyl-2-pyrrolidone) (PVP) showed the highest activity compared with those of the particles reduced by other reductants. PVP/Ru molar ratio and reaction temperature were two key factors responsible for the stability and activity of the catalysts. With a PVP/Ru molar ratio of 40, Ru nanoparticles kept an almost steady space-time yield (STY) of C_{5+} hydrocarbons 0.51 g-C_{5+} g-cat^{-1} h^{-1} throughout 240 h running at 150 °C. The size of Ru nanoparticles grew very slightly from 2.0 nm before the reaction to 2.2 nm after the reaction. X-ray photoelectron spectroscopy, Fourier transform infrared spectroscopy, and Gel Permeation Chromatography were used to reveal the structural information of the catalysts before and after reaction, and the characterization results were correlated with the catalytic performances.

1. Introduction

Syngas, a mixture of CO and H_2, can be transformed to liquid fuels via Fischer–Tropsch synthesis (FTS) [1,2]. FTS is believed to be an important process in the post petroleum era but only partly industrialized in a handful of companies due mainly to its poor energy and economic efficiencies. Zong and co-workers used hydrothermal treatment of glucose and iron nitrate to synthesis a new Fe*x*O*y*@C sphere catalyst which revealed remarkable stability and selectivity [3]. By confining iron in the nanotube, Bao et al. found that the catalysis activity was notably increased and the yield of C_{5+} hydrocarbons was twice that over the outside iron catalyst [4]. We have recently demonstrated that poly(N-vinyl-2-pyrrolidone) (PVP) stabilized Ru nanoparticles in aqueous phase FTS shows a 35-fold increase in activity over traditional supported Ru catalyst at an operating temperature of 150 °C and a 16-fold increase at only 100 °C [5], bringing a more efficient route to produce hydrocarbon fuels. A high activity was then achieved in polyethylene glycol phase, a green solvent, by using Fe nanoparticles as catalyst [6]. The excellent catalytic activities are originated not only from their high surface area when the diameter of the nanoparticles is smaller than 5 nm, but also from that the nanoparticles are homogeneously dispersed in liquid phase and therefore three dimensionally rotational in nature [7]. It is worthy to note that the hydrocarbon product does not mix with water and polyethylene glycol, so the resulting fuel is easily separated with the catalysts. Therefore, a demonstration for the liquid phase FTS process carried out in a continuous flow system is a crucial step for an industrial consideration.

In fact, the reactor design is always an important issue for conventional FTS processes [8–11]. Fixed bed, fluidized bed, slurry phase reactors, and even microchannel reactor were widely investigated to increase the efficiencies of FTS [12–16]. Methane formation and catalyst deactivation could be influenced a lot by the hot spot in the reactor because FTS is a high exothermal process. Slurry reactor is attractive for FTS because the heat and product formed during reaction could be removed continuously by the solvent [17,18].

Herein, we investigated the FTS catalyzed by aqueous phase Ru nanoparticles in detail, and established a stirred tank slurry reactor to demonstrate the potential of recycling and scale-up abilities of the soluble metal nanoparticles system. Details about the PVP (PVP molecular weight and PVP/Ru molar ratio), the reaction temperature, and the effect of the reaction on the Ru nanoparticles and PVP stabilizer were also studied. To our best knowledge, it is the first time to report such a soluble nanoparticle catalytic system in a continuous flow reactor.

2. Experimental

2.1. Catalyst preparation

2.1.1. Nanoparticles synthesis via H_2 reduction [5]

Aqueous solution of PVP stabilized Ru nanoparticles were prepared from the reduction of $RuCl_3 \cdot nH_2O$ in the presence of PVP

* Corresponding author. Tel.: +86 10 62758603; fax: +86 10 62758603.
E-mail address: dma@pku.edu.cn (D. Ma).

0920-5861/$ – see front matter © 2011 Elsevier B.V. All rights reserved.
doi:10.1016/j.cattod.2011.09.040

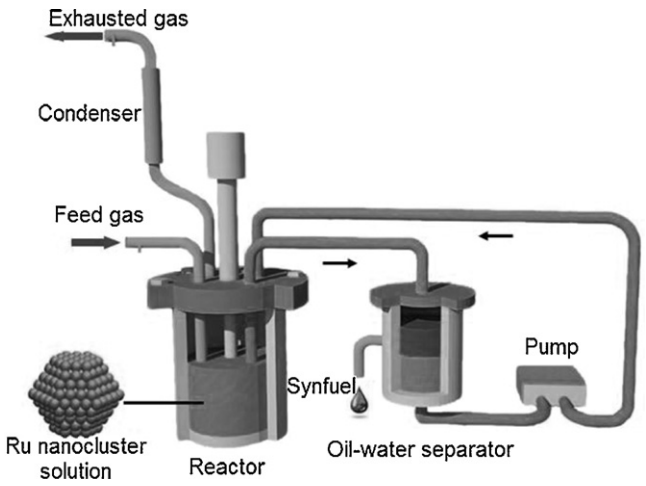

Scheme 1. Scheme of continuous flow reactor for the aqueous phase FTS.

of different molecular weights. In a typical procedure, $RuCl_3 \cdot nH_2O$ (75 mg, 2.79×10^{-4} mol Ru) and PVP (*K*30, 1.24 g, PVP/Ru = 40, where the ratio was the mole of PVP monomer units to ruthenium mole) were added into a beaker containing 20 ml deionized water. The solution was transferred and reacted in a 60 ml autoclave under 2 MPa H_2 at 150 °C for 2 h with a stirring speed of 800 rpm. For the large scale catalyst testing, 1.64 g $RuCl_3 \cdot nH_2O$ and 27.90 g PVP were mixed in 450 ml water. The solution was then reacted under 3 MPa H_2 at 150 °C for 4 h.

2.1.2. Nanoparticles synthesis via ethylene glycol reduction [19]

Typically, $RuCl_3 \cdot nH_2O$ (73 mg) and PVP (1.24 g) were dissolved in ethylene glycol (20 ml) under stirring and refluxed for 2 h to prepare Ru nanoparticles. After cooling down to room temperature, the solution was dialyzed against deionized water for several times to ensure ethylene glycol all was removed.

2.1.3. Nanoparticles synthesis using $NaBH_4$

$RuCl_3 \cdot nH_2O$ (73 mg) and PVP (1.24 g) were dissolved in 10 ml water, and then sodium borohydride (0.20 g) dissolved in 5 ml water was added very quickly under vigorous stirring. The solution was stirred for 1 h, and then dialyzed in water to remove remaining ions.

2.2. Catalytic reaction

Two types of reactors were used to evaluate the catalysts.

(1) Catalyst screening was carried out in a 60 ml autoclave. A solution of Ru nanoparticles was placed in the autoclave with 3.0 MPa syngas ($CO/H_2 = 1/2$). After reaction for 6 h at 150 °C under stirring of 800 rpm, the autoclave was put into cold water to quench the reaction. Products were analyzed by Fourier transform infrared spectroscopy (FT-IR), GC and GC–MS, as described in details in our previous work [5].
(2) Scheme 1 shows the stirred tank slurry reactor. Feed gas ($CO/H_2/Ar = 32/64/4$) was continuously introduced into the bottom of the reactor with a stainless steel tube. Gas products were released from the system through a water condenser where liquid products and water vapor being separated prior to the exit of the gases. A thermocouple inserted into the aqueous phase was used to monitor the reaction temperature and a back pressure valve was used to keep the reaction pressure at 3.0 MPa. The gas products were analyzed by an on-line Agilent gas chromatography and an FT-IR spectrometer. An Agilent HP-MOLESIEVE column with TCD was used to analyze CO, Ar and CH_4. The conversion of CO was calculated as follows:

$$\text{CO conversion} = 100 \times \frac{X_{in} - X_{out}}{X_{in}}$$

where the X_{in} and X_{out} are the flow rate of CO in the inlet gas and the effluent gas, respectively. Ar was used as an internal standard to calculate the ratio of X_{out} to X_{in}. Another HP-AL/M column with FID was used to analyze C_1–C_4 hydrocarbons. CH_4 was used to combine the analysis results from TCD and FID. CO_2 was analyzed by FT-IR spectrometer. The liquid product mixture could be pumped into an oil-water separator, where the organic phase was released while the water phase containing the catalysts was pumped back to the main reactor. After the reaction, 100 ml HPLC grade cyclohexane or toluene was piped into the reactor and refluxed at 150 °C for 2 h. The organic phase was analyzed by GC equipped with a 60 m HP-5 column.

2.3. Catalyst characterization

For transmission electron microscopy (TEM) observation, aqueous Ru nanoparticle solution was dispersed under ultrasonication for 2 h, and then one drop of solution was placed onto a copper grid coated with a polymer or carbon film. A Philips Tecnai F30 transmission electron microscope operating at 300 kV was used to observe the Ru nanoparticles. The particle size distribution was counted with at least 300 particles.

For X-ray photoelectron spectroscopy (XPS) characterization, after adding 8 ml acetone into 10 ml aqueous solution of Ru nanoparticles, the sample was centrifuged. The solid was washed with deionized water several times to remove most of the PVP on the surface of the nanoparticles, and then dried under vacuum at 60 °C. XPS spectra was measured using an AlKa (1486.7 eV) X-ray source, with the pressure of the measuring chamber set at 5×10^{-9} Torr. C1s binding energy was set to 284.8 eV as a reference.

For FT-IR measurements, the aqueous solution containing the catalysts was dried under vacuum to remove water, and then dried sample was mixed with KCl. The spectrum was measured on a Bruker Vector 22 FT-IR spectrometer with a resolution of 2.0 cm^{-1}.

The weight-average molecular weight (Mw) of the PVP samples was determined on an Agilent Gel Permeation Chromatography (GPC) using N,N-dimethylformamide (DMF) as mobile phase. Polystyrene was used as a standard sample and Mw was calculated based on the standard curve.

3. Results and discussion

3.1. Catalysts screening

Table 1 shows the catalytic activity of Ru nanoparticles prepared by different reduction methods in the presence of PVP. The screening reactions were conducted at 150 °C in a 60 ml autoclave for 6 h. Three different reduction methods were used to prepare Ru nanoparticles. The catalyst prepared by $NaBH_4$ reduction method showed much lower activity (entry 1) compared with the catalysts prepared by the others. We demonstrated previously that FTS activity was sensitive to the particle size of Ru catalyst [5]. However, as the sizes of the nanoparticles prepared by all three methods were similar to each other, i.e., around 2 nm, the low activity of the catalyst prepared by $NaBH_4$ reduction method might be due to the presence of B in the system. The catalyst prepared by ethylene glycol reduction had a similar average turnover frequency (ATOF) (entry 2) compared with the catalyst prepared by H_2 reduction. We also prepared Ru nanoparticles in the presence of PVP of different *K* values (*K*15, *K*30, and *K*90). The *K* value is a function of average

Table 1
Activity of Ru catalysts prepared with different reductants and stabilizers.

Entry[a]	Reduction reagent	Type of PVP	Diameter before reaction (nm)	ATOF ($mol_{CO} mol_{Ru}^{-1} h^{-1}$)	Diameter after reaction (nm)
1	$NaBH_4$	*K*30	1.8 ± 0.4	1.6	2.0 ± 0.6
2	Glycol	*K*30	2.0 ± 0.3	6.5	2.1 ± 0.4
3[b]	H_2	*K*30	2.0 ± 0.2	6.9	2.1 ± 0.2
4	H_2	*K*90	1.8 ± 0.4	5.2	1.8 ± 0.5
5	H_2	*K*15	2.0 ± 0.3	5.9	Aggregate

[a] Reaction conditions: 3.0 MPa syngas (CO/H_2 = 1/2), 150 °C, 6 h, stirring speed of 800 rpm, PVP/Ru = 40/1, 20 ml solvent, 2.79×10^{-4} mol Ru.
[b] Data from Ref. [3].

molecular weight, reflecting the degree of polymerization and tuning the intrinsic viscosity for PVP [20,21]. Entries 3–5 in Table 1 show that the catalysts prepared under the protection of PVP having different *K* values had very similar particle size around 2.0 nm, and thus they had very similar initial catalytic activity. However, after 6 h running at 150 °C, serious aggregation occurred for the Ru nanoparticles protected by lower *K* value PVP (*K*15) while no change in particle size was observed for the particles protected by higher *K* value PVPs (*K*30, *K*90). It is also interesting to note that the activity of the catalyst in the presence of the highest *K* value PVP (*K*90) was slightly lower than the catalyst stabilized by that of *K*30, suggesting that there was a balance between the catalyst activity and the stability, i.e., too strong protection of PVP may block the route for the reactant to diffuse onto and react over the metal surface, and thus lead to an inferior catalytic activity.

The molar ratio of PVP/Ru also had an effect on the activity of the catalysts. As shown in Fig. 1, when PVP/Ru = 10 (*K*30, it was used throughout the manuscript unless stated specifically), the activity of the catalyst was 5.8 $mol_{CO}\ mol_{Ru}^{-1}\ h^{-1}$. By increasing the PVP/Ru molar ratio from 20, 40 to 120, the activity decreased slightly and almost monotonically, to 160, the activity of the catalyst suddenly dropped to 3.4 $mol_{CO}\ mol_{Ru}^{-1}\ h^{-1}$. This could be explained that higher concentration of PVP, similar to the use of PVP of high molecular weight, would increase the viscosity of the reaction mixture, making the diffusion more slowly and leading to a low catalytic activity.

3.2. FTS in a continuous flow reactor

Although one-pot batch reactor can be used to investigate the catalytic performance of different catalysts, the reaction operated in a continuous mode is much more important from industrial point of view. Therefore, we established a stirred tank slurry reactor system, as illustrated in Scheme 1, where the syngas can be fed into reactor continuously, while the product mixture can be withdrawn from the reactor then be separated with the catalyst. To check whether Ru nanoparticles can keep the outstanding performance during the long-time running in this mode, we conducted series of experiments under different reaction conditions. Fig. 2 shows CO conversion over Ru catalysts stabilized by different amount of PVP. Clearly, PVP/Ru molar ratio played an important role in the stability of the catalyst. With PVP/Ru molar ratio in the range of 20–80, all the Ru nanoparticle catalysts presented a high CO conversion (over 80%) at the beginning. However, when the ratio was lowered to 10, the catalyst reached the maximum (89%) at the 72nd h, and then dropped very quickly in further 80 h. After about 160 h running, CO conversion remained was only 14%. By increasing the PVP/Ru molar ratio to 20, the stability of the catalyst increased significantly. The best ratio was 40, i.e., even after 240 h running of the same catalyst, the CO conversion was still about 70%. It can be seen from Fig. 2 that the catalyst having a PVP/Ru molar ratio of 80 gave a conversion about 5% lower than those of the best one throughout the 240 h running, indicating that very strong stabilization was not necessarily a good approach.

We also investigated the influence of temperature on the reaction of Ru nanoparticles with a PVP/Ru molar ratio of 40. With a feed gas flow rate of 40 ml/min, Ru nanoparticle catalysts showed the best balance between activity and stability at 150 °C compared with the performances at other investigated temperatures. As shown in Fig. 3a, at 150 °C, the conversion of CO increased slightly from 74% at the beginning to 83% after 80 h running, and then dropped to 68% after 240 h running. On the one hand, at a lower temperature, e.g., 130 °C and 140 °C, although the catalyst was quite stable with no more than 10% difference in CO conversion after the running for 240 h, the conversion itself was too low, only around 10% and 30%, respectively. On the other hand, when raising the temperature to 160 °C and 170 °C, the catalyst became very active, the pressure

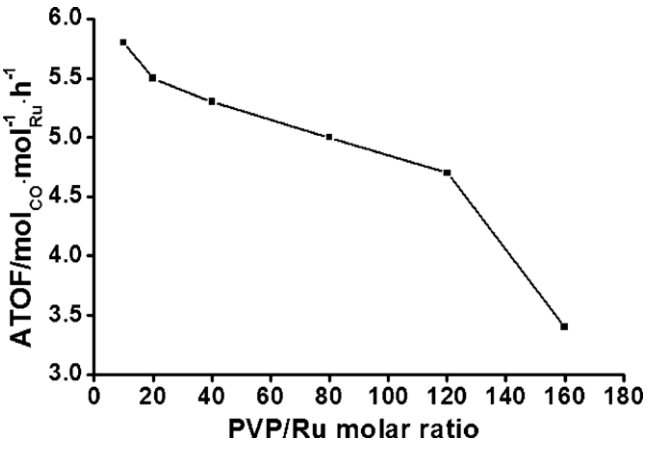

Fig. 1. Effect of PVP/Ru molar ratio on the catalytic activity of the Ru nanoparticles. Reaction conditions: 450 ml catalyst solution, 6.1×10^{-3} mol Ru, 3.0 MPa syngas (CO/H_2 = 1/2), 150 °C, 6 h, stirring speed of 1000 rpm.

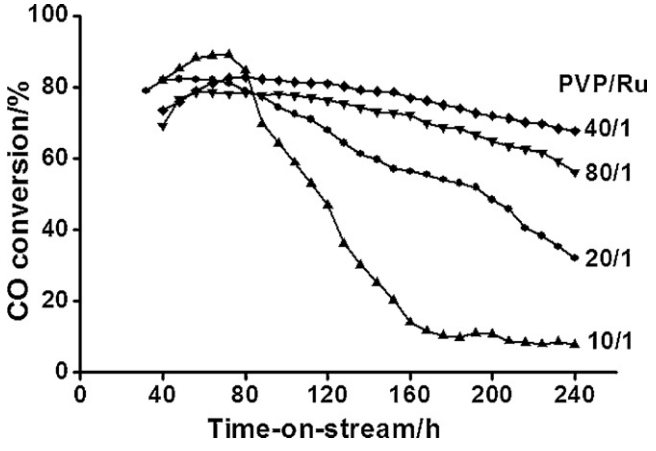

Fig. 2. Time-on-stream of CO conversion on Ru nanoparticles with different PVP/Ru molar ratio. Reaction conditions: 450 ml catalyst solution, 6.1×10^{-3} mol Ru, 3.0 MPa syngas ($CO/H_2/Ar$ = 32/64/4), stirring speed of 1000 rpm, feed gas flow rate: 40 ml/min.

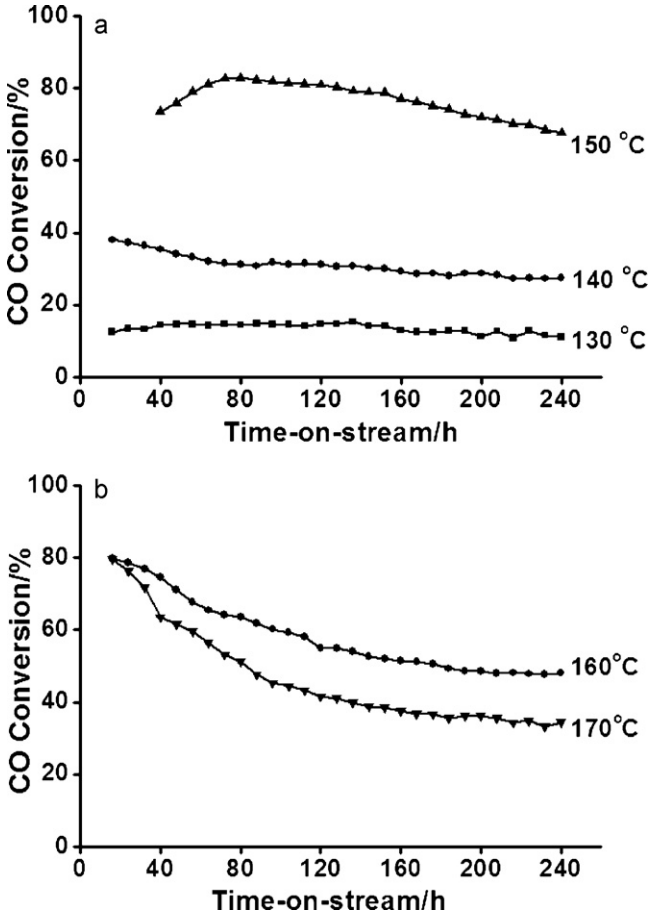

Fig. 3. Time-on-stream of CO conversion on Ru nanoparticles at different temperatures. Reaction conditions: 450 ml catalyst solution, 6.1×10^{-3} mol Ru, PVP/Ru = 40/1, 3.0 MPa syngas ($CO/H_2/Ar$ = 32/64/4), stirring speed of 1000 rpm. (a) Feed gas flow rate: 40 ml/min. (b) Feed gas flow rate were 73 ml/min and 100 ml/min at 160 °C and 170 °C, respectively.

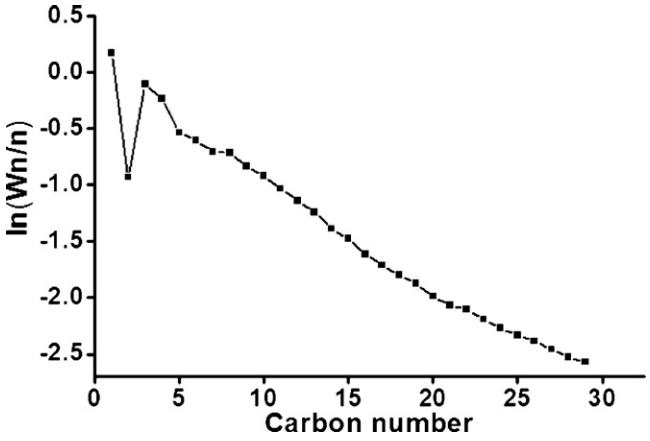

Fig. 4. Anderson–Schultz–Flory plot for the distribution of hydrocarbon products over the Ru catalyst (PVP/Ru = 40) after reacting for 240 h at 150 °C.

of syngas, which was 3.0 MPa at the beginning, dropped down very quickly under the feed gas flow rate of 40 ml/min, resulting in no gas product exiting from the reactor. Therefore, we increased the feed gas flow rate to 73 ml/min at 160 °C, and to 100 ml/min at 170 °C, respectively, to guarantee that the reactor system was under continuous flow conditions. It can be seen from Fig. 3b that the CO conversions obtained at the beginning were about 80%, which was similar to the conversion obtained at 150 °C under the flow rate of 40 ml/min. However, the CO conversions dropped down quickly, after 80 h running, the conversion remained at 160 °C was 64%, and the conversion remained at 170 °C was only about 51%, indicating a fast deactivation of the catalysts at 160 °C and 170 °C. The deactivation could be attributed to the hydrogenation/degradation of the stabilizer and the nature of instability of nanoparticles.

Fig. 4 shows the product distribution of FTS operated in the continuous flow mode after 240 h running at 150 °C at a feed gas flow rate of 40 ml/min. It is noteworthy that the product distribution agreed well with the Anderson–Schulz–Flory statistics. The chain growth probability factor α, calculated from the slope of the line, was 0.91, indicating that more high molecular weight products were obtained compared with those obtained on traditional supported Ru catalysts [22–25]. This was perhaps due to the lower temperature and higher pressure employed in our reaction conditions, which both benefited the chain growth during the reaction. The selectivity towards CH_4 and CO_2, the ratios of olefin to paraffin, ATOF, and space-time yield (STY) of C_{5+} hydrocarbons are summarized in Table 2. The methane selectivity was no higher than 3% observed for all the reaction temperatures evaluated while the selectivity of CO_2, which was 3.2% at 150 °C, increased with the reaction temperature. A rather high CO_2 selectivity of 4.5% was obtained at 170 °C. This might be resulted from the presence of aqueous phase, which is beneficial for the well-known water-gas-shift (WGS) reaction especially at higher reaction temperature. The decrease in olefin to paraffin ratio was a result of higher hydrogenation activity of the catalyst at higher temperatures. It can be seen after 240 h running that ATOF obtained at 150 °C reached 4.1 $mol_{CO}\ mol_{Ru}^{-1}\ h^{-1}$, which was comparable with the result obtained from the static mode (5.5 $mol_{CO}\ mol_{Ru}^{-1}\ h^{-1}$, see Fig. 1). The average STY of C_{5+} after 240 h running at 150 °C was 0.51 g-C_{5+} g-$cat^{-1}\ h^{-1}$ which was above 5 times higher than that over a traditional catalyst at 200 °C in the presence of 4.54 bar water vapor [22].

3.3. Catalysts characterization

TEM, XPS, FT-IR and GPC were used to characterize the Ru nanoparticle catalyst before and after 240 h running at 150 °C with a total feed gas flow rate of 40 ml/min in the continuous flow mode. Fig. 5 shows the TEM images and size distributions of Ru nanoparticles as prepared with a PVP/Ru molar ratio of 40 before and after reaction. It is observed from TEM that the Ru nanoparticles prepared by hydrogen reduction method presented a nanowire-like structure, which was formed by connecting individual Ru nanoparticles. It can be found that the size distributions of Ru nanoparticles after reaction increased slightly from 2.0 ± 0.2 nm at the beginning to 2.2 ± 0.4 nm at the end, indicating the catalyst were quite stable under this reaction condition.

Fig. 6 presents the X-ray photoelectron spectra of the catalysts before and after reaction. As shown in Fig. 6a, peaks appeared at 284.8, 285.2, 285.9 and 287.7 eV could be attributed to different carbon atoms of PVP [26,27]. The peak at 280.2 eV was attributed to Ru metal's $3d_{5/2}$ peak, while the others at 280.9 eV and 282.2 eV were originated from different oxide states of Ru components [28]. These very small amounts of Ru oxidation components were thought to be produced during the sampling and transferring in air. After the reaction, the peak at 284.8 eV dominated the spectrum (Fig. 6b). This peak could be assigned to the FT wax adhering on the surface of the catalysts. The wax formed during the reaction was difficult to be removed during the sample preparation process.

FT-IR has also verified the existence of wax on the catalysts (Fig. 7). It is clear that the spectrum, Fig. 7a, of the used catalyst after reaction was an overlap of those of fresh catalyst (Ru/PVP,

Table 2
Catalytic performance of Ru catalysts for the Fischer–Tropsch synthesis.

Temp. (°C)	CH_4 sel. (%)	CO_2 sel. (%)	O/P[b]	ATOF ($mol_{CO} mol_{Ru}^{-1} h^{-1}$)	C_{5+}STY/g cat-$g^{-1} h^{-1}$
130[a]	1.4	1.8	0.59	0.8	0.10
140[a]	1.4	2.9	0.41	1.9	0.24
150[a]	1.6	3.2	0.40	4.1	0.51
160[c]	2.2	3.4	0.35	5.6	0.69
170[d]	2.6	4.5	0.32	6.6	0.81

[a] Reaction conditions: 450 ml catalyst solution (water containing Ru nanoparticles), 6.1×10^{-3} mol Ru, PVP/Ru = 40/1, 3.0 MPa syngas ($CO/H_2/Ar$ = 32/64/4), 40 ml/min feed gas flow rate and stirring speed of 1000 rpm for 240 h.
[b] Olefin/paraffin ratio in C_2–C_4 hydrocarbon products (O: olefin; P: paraffin).
[c] Reaction conditions were the same as a except that the feed gas flow rate was 73 ml/min.
[d] Reaction conditions were the same as a except that the feed gas flow rate was 100 ml/min.

Fig. 7b) and F-T wax (Fig. 7c). As the wax was formed on the surface of the Ru catalyst, unavoidably, some of the wax which did not diffuse into the aqueous phase in the reaction system would stay with the catalysts.

We also investigated the structural information of PVP after the reaction. When we simulated the high temperature treatment of PVP (same pH value as used for the reaction mixture, but the Ru nanoparticles were not added as it will disturb Gel Permeation Chromatograph measurement), Mw of PVP was relatively stable at 150 °C for 300 h. It can be seen from Fig. 8 that Mw dropped from 17.3 kDa to 11.5 kDa at the first 50 h and then kept almost steady afterward.

From the characterization results obtained we can conclude that with a PVP/Ru molar ration of 40, Ru nanoparticles prepared by hydrogen reduction was quite stable during 240 h running under the reaction condition of 150 °C with a total feed gas flow rate of 40 ml/min.

Ru nanoparticle stabilized by PVP could aggregate under certain circumstance, e.g., high reaction temperature (Table S1), during the reaction. Two factors possibly contributed to the aggregation at an elevated temperature. The most important one might be the hydrolysis or hydrogenolysis of PVP during the high temperature reaction. It can be seen from Fig. S1, after 300 h pretreatment, the Mw of PVP decreased slightly for the samples treated in the range

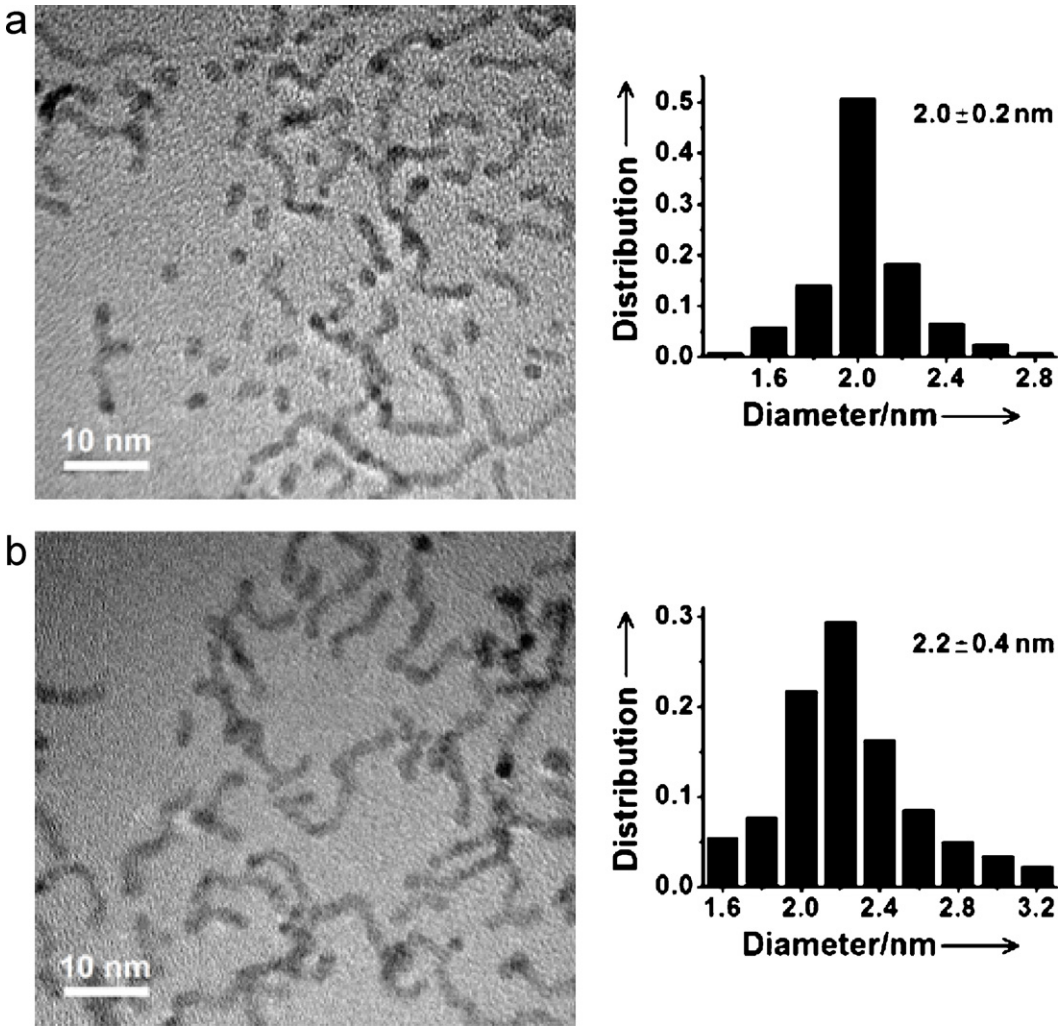

Fig. 5. TEM images and diameter distributions for Ru nanoparticles stabilized with PVP/Ru = 40/1 before (a) and after (b) reaction.

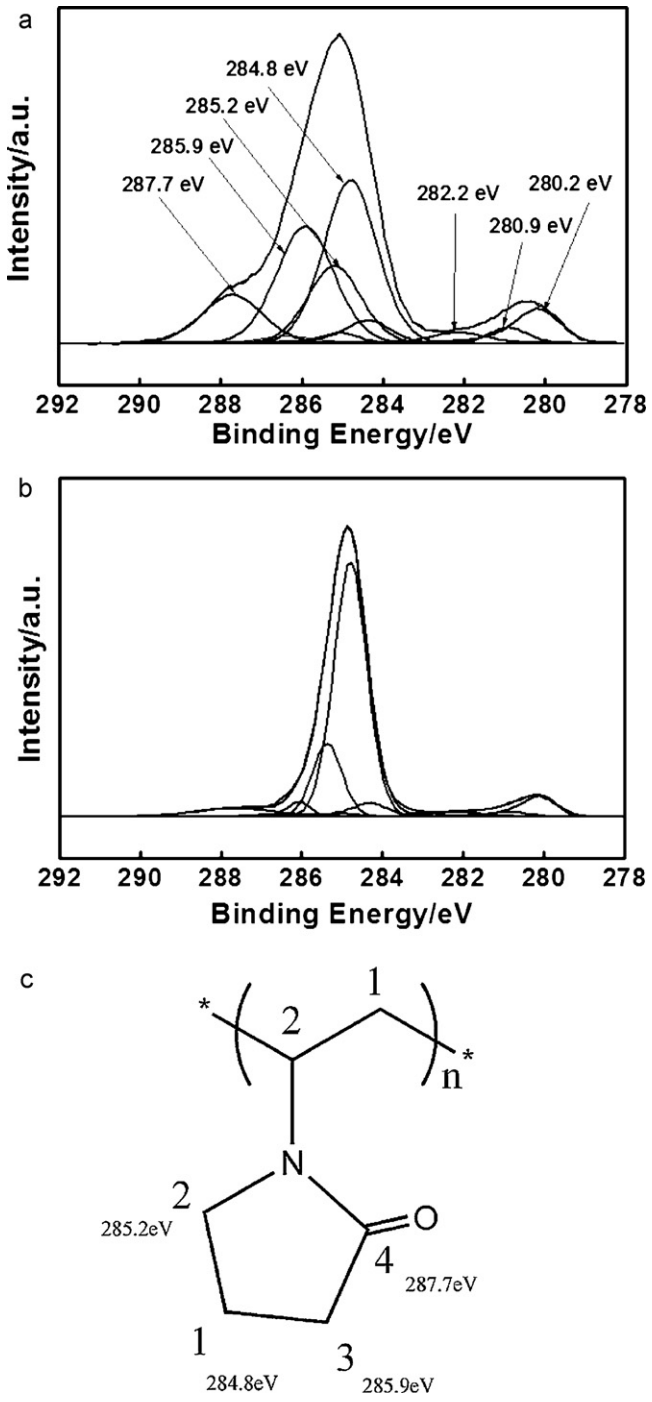

Fig. 6. X-ray photoelectron spectra of catalyst before (a) and after (b) reaction, (c) configuration of PVP repeated unit.

of 130–150 °C but dropped significantly for the samples treated at 160 and 170 °C, especially for the sample at 170 °C. The decrease of PVP's molecular weight weakened the stabilization effect of PVP over the discrete metal nanoparticles. It will eventually lead to the formation of large aggregates of Ru nanoparticles to obtain a smaller surface energy. Together with the weakening of stabilization effect of the broken PVP fragments, the high molecular weight products (the second factor) such as wax may adhere on the Ru/PVP interface. The wrapping of Ru nanoparticle by FTS wax could reduce the stabilization effect of PVP during the reaction.

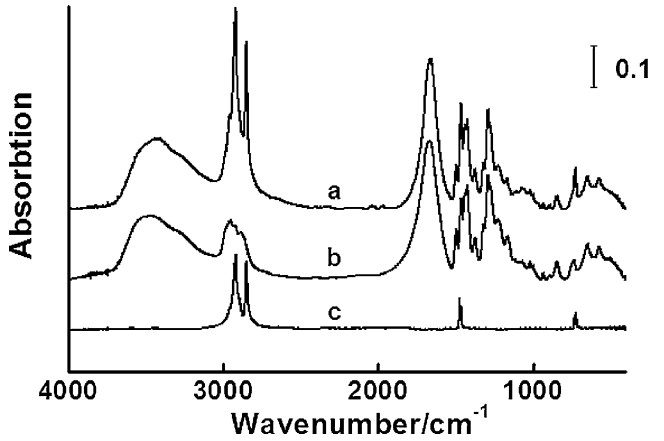

Fig. 7. FT-IR spectra of (a) Ru-PVP after reaction, (b) Ru-PVP before reaction, (c) F-T wax.

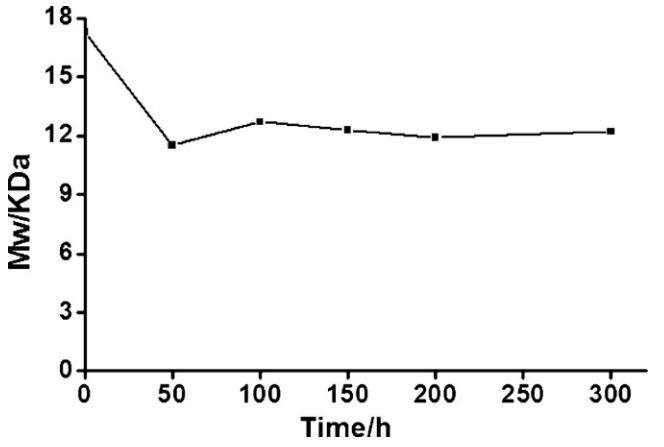

Fig. 8. Change of molecular weight of PVP with time at 150 °C in the acidic water. 1.24 g PVP was dissolved in deionized water with 0.08 g 37% HCl (equal to the mole of HCl from the reduction of $RuCl_3 \cdot nH_2O$). The solution was heated to 150 °C under 1 MPa syngas in autoclave for 300 h.

4. Conclusions

Aqueous phase Fischer–Tropsch synthesis conducted in a continuous flow mode, a crucial step for the feasibility demonstration in an industrial consideration, has successfully realized for the first time. Hydrogenation reduction is an easy and effective method for the preparation of aqueous phase Ru nanoparticle catalyst. The best result of space time yield obtained at 150 °C with a PVP/Ru molar ratio of 40 and a feed gas flow rate of 40 ml/min was 0.51 g-C_{5+} g-cat^{-1} h^{-1}. Catalysts characterizations showed that the size of the Ru nanoparticles (2.0–2.2 nm) kept almost unchanged after the reaction, demonstrating a successful long life performance for the noble metal nanoparticle catalyst dispersed in liquid phase operated in a continuous flow mode.

Acknowledgements

This work was financially supported by the Ministry of Science and Technology of China (2011CB201402) and the Beijing Municipal Natural Science Foundation (2102026).

Appendix A. Supplementary data

Supplementary data associated with this article can be found, in the online version, at doi:10.1016/j.cattod.2011.09.040.

References

[1] F. Fischer, H. Tropsch, Brennst. Chem. 4 (1923) 276.
[2] F. Fischer, H. Tropsch, Brennst. Chem. 7 (1926) 97.
[3] G. Yu, B. Sun, Y. Pei, S. Xie, S. Yan, M. Qiao, K. Fan, X. Zhang, B. Zong, J. Am. Chem. Soc. 132 (2010) 935.
[4] W. Chen, Z. Fan, X. Pan, X. Bao, J. Am. Chem. Soc. 130 (2008) 9414.
[5] C.X. Xiao, Z.P. Cai, T. Wang, Y. Kou, N. Yan, Angew. Chem. Int. Ed. 47 (2008) 746.
[6] X.B. Fan, Z.Y. Tao, C.X. Xiao, F. Liu, Y. Kou, Green Chem. 12 (2010) 795.
[7] D. Zhao, M. Wu, Y. Kou, E.Z. Min, Catal. Today 74 (2002) 157.
[8] B.H. Davis, Catal. Today 71 (2002) 249.
[9] C.N. Satterfield, G.A. Huff, Chem. Eng. Sci. 35 (1980) 195.
[10] D. Stern, A.T. Bell, H. Heinemann, Chem. Eng. Sci. 38 (1983) 597.
[11] R. Guettel, U. Kunz, T. Turek, Chem. Eng. Technol. 31 (2008) 746.
[12] M.E. Dry, Appl. Catal., A 138 (1996) 319.
[13] S.T. Sie, R. Krishna, Appl. Catal., A 186 (1999) 55.
[14] D.J. Duvenhage, T. Shingles, Catal. Today 71 (2002) 301.
[15] Y.Y. Liu, T. Hanaoka, T. Miyazawa, K. Murata, K. Okabe, K. Sakanishi, Fuel Process. Technol. 90 (2009) 901.
[16] C.S. Cao, J.L. Hu, S.R. Li, W. Wilcox, Y. Wang, Catal. Today 140 (2009) 149.
[17] V. O'Shea, M.C. Alvarez-Galvan, J.M. Campos-Martin, J. Fierro, Appl. Catal., A 326 (2007) 65.
[18] S.C. Saxena, M. Rosen, S.N. Smith, J.A. Ruether, Chem. Eng. Commun. 40 (1986) 97.
[19] Y. Chen, K.Y. Liew, J.L. Li, Mater. Lett. 62 (2008) 1018.
[20] Y.E. Kirsh, T.M. Karaputadze, V.I. Svergun, T.A. Sus, O.I. Sutkevich, I.I. Tverdokhlebova, V.P. Panov, Pharm. Chem. J. 14 (1980) 501.
[21] J. Swei, J.B. Talbot, J. Appl. Polym. Sci. 90 (2003) 1153.
[22] M. Claeys, E. van Steen, Catal. Today 71 (2002) 419.
[23] M.L. Turner, N. Marsih, B.E. Mann, R. Quyoum, H.C. Long, P.M. Maitlis, J. Am. Chem. Soc. 124 (2002) 10456.
[24] K. Murata, K. Okabe, I. Takahara, M. Inaba, M. Saito, React. Kinet. Catal. Lett. 90 (2007) 275.
[25] C.S. Kellner, A.T. Bell, J. Catal. 75 (1982) 251.
[26] P. Jiang, J.J. Zhou, R. Li, Z.L. Wang, S.S. Xie, Nanotechnology 17 (2006) 3533.
[27] L. Li, C.M. Chan, L.T. Weng, Polymer 39 (1998) 2355.
[28] C.D. Wagner, W.M. Riggs, L.E. Davis, F. Moulder, J.G.E. Muilenberg, Physical Electronics Division, vol. 55, Perkin-Elmer, Eden Prairie, MN, 1979, p. 344.